MONTHLY WEATHER REVIEW
VOLUME 97, NUMBER 12
DECEMBER 1969

UDC 551.509.312 : 551.511.13 : 532.13

NUMERICAL STUDIES OF EFFECTS OF SURFACE FRICTION ON LARGE-SCALE ATMOSPHERIC MOTIONS [1]

MAURICE B. DANARD
University of Waterloo, Waterloo, Ontario, Canada

ABSTRACT

A simple relationship is obtained between pressure changes associated with friction and the geostrophic drag coefficient. From this, the imbalance between frictionally induced mass inflow and outflow is shown to be one or two orders of magnitude smaller than either the inflow or outflow.

Numerical integrations using the primitive equations are performed for an axially symmetric autobarotropic low-pressure system. The velocity components and pressure tendencies are found to depend critically on the drag coefficient.

Two actual synoptic cases are studied using a quasi-geostrophic numerical model incorporating release of latent heat. Computations are performed with and without surface friction. When friction is excluded, the 1000-mb Highs and Lows are more intense.

Two methods of computing the surface stress are compared. One is based on variations in terrain height and the other on the nature of the vegetation. Differences are large, especially over the western part of North America.

1. INTRODUCTION

An accurate computation of the stress (force per unit area) at the interface between atmosphere and earth is desirable for many reasons. Wind speeds and vertical motions in the Ekman layer (planetary boundary layer) depend critically on the surface stress. The frictionally induced vertical velocity contributes to low cloudiness and precipitation. If the atmosphere is conditionally unstable, this forced ascent will facilitate development of convective clouds. In addition, the importance of Ekman layer frictional influences in long-range forecasting and the general circulation is easily demonstrated (see, for example, fig. 7B1 of Smagorinsky and others, 1965, or Kung, 1968). Other influences are described below.

It is readily shown that, if there were no compensating mass outflow aloft, the frictional convergence in the Ekman layer in cyclones would result in pressure rises far in excess of those observed. The mass outflow must almost, but not quite, balance the mass inflow. In section 2, a simple relation between the pressure tendency and the geostrophic drag coefficient is derived. This permits a comparison of the magnitudes of the mass outflow or inflow and their sum (that is, the net inflow).

In section 3, an axially symmetric autobarotropic low-pressure system is studied by integrating the primitive equations of motion. The pressure tendencies, wind components, and vertical velocities are found to depend critically on the drag coefficient. From a survey of the literature, Sawyer (1959) suggests the following values for the drag coefficient:

$$\text{over sea } 5\times10^{-4}$$
$$\text{over land generally } 1\times10^{-2},$$
and
$$\text{over mountainous country } 3\times10^{-2}.$$

The value for over the sea is somewhat smaller than proposed by Sheppard (1958) of about 2×10^{-3}. Nevertheless, the range in drag coefficient suggests that observed changes in cyclones when moving over a surface of varying roughness (land to sea) may be due, in part, to variations in surface stress.

The role of surface friction in the development of hurricanes has recently received considerable attention. Charney and Eliassen (1964) have suggested that surface friction may accelerate the growth of tropical cyclones in the early stages. This is due to moisture supply and subsequent release of latent heat arising from frictional convergence. The importance of this effect was also recognized by Ooyama (1964). Kuo (1965) derived a relation between moisture convergence and release of latent heat in cumulus clouds. Krishnamurti (1968) adapted Kuo's results into a tropical numerical forecasting model. However, release of latent heat is also important in the development of extratropical cyclones (Danard, 1964, 1966*a*, *b*).

[1] A summary of sections 3 and 4 of this paper was presented at the Stanstead Seminar, Stanstead, Quebec, July 21–Aug. 1, 1969.

Graystone (1962) studied effects of surface friction with a two-level quasi-geostrophic numerical model. Released latent heat was not included. In a 24-hr forecast, the central 1000-mb height of a cyclone was raised 150 m by including friction. Bushby (1968) performed calculations with a 10-level primitive equations model including release of latent heat and friction. In one case study, the magnitude of the 24-hr-forecast vertical velocities at 900 mb was increased by more than 10 mb hr^{-1} as a result of incorporating surface friction. However, the maximum rainfall rates were relatively unaffected. In another case, the inclusion of friction raised the 24-hr predicted central pressure of a sea-level Low by 16 mb. In section 4, comparative 36-hr numerical integrations, with and without surface friction, are made for two synoptic cases of midlatitude cyclogenesis. The model (Danard, 1966*a*,*b*) incorporates effects of released latent heat. The friction-free prognoses give more intense Highs and Lows at 1000 mb than do the forecasts with surface friction. However, surface friction has little effect on predicted precipitation amounts.

When surface stress is incorporated into numerical weather prediction models (for example, Shuman and Hovermale, 1968), use is often made of the geostrophic drag coefficients provided by Cressman (1960). These drag coefficients depend on variations in terrain height. However, a different approach has been followed by Lettau (1962) and Kung (1966). In their computations, vegetation, rather than undulations in topography, determines the magnitude of the stress. Some support for this postulate is provided by Holopainen (1963) who estimates that half the frictional energy dissipation in the lowest kilometer occurs below the anemometer level. In section 5, the surface stress is computed by the two methods described above. Since the disparities between the two calculations are large, it is concluded that the computation of surface stress needs further investigation.

2. A SIMPLE RELATION BETWEEN THE PRESSURE TENDENCY AND THE DRAG COEFFICIENT

Ignoring horizontal eddy diffusion, the equation of motion may be written

$$\mathbf{V}=\mathbf{V}_g+\frac{1}{f}\mathbf{k}\times\left(\frac{\partial\mathbf{V}}{\partial t}+\mathbf{V}\cdot\nabla_H\mathbf{V}+w\frac{\partial\mathbf{V}}{\partial z}-\frac{1}{\rho}\frac{\partial\boldsymbol{\tau}}{\partial z}\right) \tag{1}$$

where $\mathbf{V}$ and $\mathbf{V}_g$ denote the horizontal and geostrophic winds, f is the Coriolis parameter, $w=dz/dt$ the vertical velocity, ρ the density, and $\boldsymbol{\tau}$ the stress on a horizontal surface. In order to delineate the effects of friction, equation (1) will be linearized and $\partial\mathbf{V}_g/\partial t$ substituted for $\partial\mathbf{V}/\partial t$:

$$\mathbf{V}=\mathbf{V}_g+\frac{1}{f}\mathbf{k}\times\left(\frac{\partial\mathbf{V}_g}{\partial t}-\frac{1}{\rho}\frac{\partial\boldsymbol{\tau}}{\partial z}\right). \tag{2}$$

The pressure tendency at the earth's surface (assumed flat) is given by

$$\frac{\partial p_0}{\partial t}=-\int_0^\infty g\nabla_H\cdot\rho\mathbf{V}dz. \tag{3}$$

Horizontal variations in ρ and f will be neglected, and $\partial\mathbf{V}_g/\partial t$ will be assumed independent of height. This would be true in a hydrostatic autobarotropic atmosphere (section 3). Substituting equation (2) in (3) then yields

$$\frac{\partial p_0}{\partial t}=\frac{p_0}{\rho_0 f^2}\nabla_H^2\frac{\partial p_0}{\partial t}+\frac{g}{f}\mathbf{k}\cdot\nabla_H\times\boldsymbol{\tau}_0 \tag{4}$$

where $\boldsymbol{\tau}_0$ is the stress exerted by the atmosphere on the earth's surface.

Consider the ageostrophic terms in equation (2). If, for example, the pressure gradient is weakening, the term $f^{-1}\,\mathbf{k}\times\partial\mathbf{V}_g/\partial t$ is directed towards higher pressure. The term $-(f\rho)^{-1}\,\mathbf{k}\times\partial\boldsymbol{\tau}/\partial z$ is of importance in the Ekman layer. If $\partial\boldsymbol{\tau}/\partial z$ is in the opposite direction to $\mathbf{V}_g$, this term is directed towards lower pressure. These two ageostrophic terms give rise to the two terms on the right side of equation (4). At the center of a filling Low, the first term of (4) is negative, and the second is positive. These terms may be regarded as representing, respectively, effects of divergence above and convergence within the friction layer.

An estimate of $\partial p_0/\partial t$ in a typical synoptic situation may be obtained by setting $\nabla_H^2\partial p_0/\partial t=-k^2\partial p_0/\partial t$, where $k=2\pi/L$ is the wave number and L is the wavelength. Let $\boldsymbol{\tau}_0=\rho C_g V_g\mathbf{V}_g$, where C_g is the geostrophic drag coefficient and V_g is the surface geostrophic wind speed. Ignoring horizontal variations in C_g and V_g, equation (4) gives

$$\frac{\partial p_0}{\partial t}=-\frac{p_0k^2}{\rho_0 f^2}\frac{\partial p_0}{\partial t}+\frac{g\rho_0C_gV_g\zeta_g}{f} \tag{5}$$

where ζ_g is the surface geostrophic vorticity. For $p_0=$ 1000 mb, $L=3000$ km, $\rho=1.2\times10^{-3}$ gm cm^{-3}, $\zeta_g=5\times10^{-5}$ sec^{-1}, $f=10^{-4}$ sec^{-1}, $C_g=2\times10^{-3}$, and $V_g=20$ m sec^{-1}, equation (5) gives $\partial p_0/\partial t=0.22$ mb hr^{-1}. At the center of a Low, the pressure tendency is equal to the rate of change of the central pressure following the motion of the Low. Thus surface friction tends to fill cyclones, and if they are observed not to do so, this must be due to other influences.

It may be remarked that with the above values, $p_0k^2\times(\rho_0f^2)^{-1}=37$ so that the term $p_0(\rho f^2)^{-1}\nabla_H^2\partial p_0/\partial t$ in equation (4) is large in magnitude compared to $\partial p_0/\partial t$ except for very long waves. Thus the frictional convergence in the Ekman layer (last term on the right side in equation (4)) is very nearly compensated by the divergence above (first term).

A final point, which is obvious from equation (5), is that the frictionally induced pressure tendency is proportional to the drag coefficient. This will be investigated further in section 3.

3. FRICTIONALLY INDUCED CIRCULATIONS IN AN AUTOBAROTROPIC ATMOSPHERE

The equation of motion may be written

$$\frac{d\mathbf{V}}{dt}=-g\nabla z-f\mathbf{k}\times\mathbf{V}+K\nabla^2\mathbf{V}+\mathbf{F}_v \tag{6}$$

where ∇ is the isobaric gradient operator, z is the height of an isobaric surface, K is the coefficient of horizontal eddy diffusion, and $\mathbf{F}_v$ is the horizontal frictional force due to vertical mixing.

Equation (6) is applied to an axially symmetric autobarotropic low-pressure system with a smooth wall at $r=1000$ km. Cylindrical coordinates (r, θ, p) are used. For a hydrostatic autobarotropic fluid, ∇z is independent of p. The symmetry condition implies that

$$\partial\psi/\partial\theta=0 \tag{7}$$

where ψ is any scalar function. The equation of continuity takes the form

$$\frac{\partial\omega}{\partial p}+\frac{1}{r}\frac{\partial}{\partial r}(rv_r)=0 \tag{8}$$

where $\omega=dp/dt$. Equation (8) may be combined with the components of (6) to yield

$$\frac{\partial v_r}{\partial t}=-\frac{1}{r}\frac{\partial}{\partial r}rv_r^2-\frac{\partial}{\partial p}\omega v_r+\frac{v_\theta^2}{r}-g\frac{\partial z}{\partial r}+fv_\theta+K\left[\frac{1}{r}\frac{\partial}{\partial r}\left(r\frac{\partial v_r}{\partial r}\right)-\frac{v_r}{r^2}\right]+F_{rv} \tag{9}$$

and

$$\frac{\partial v_\theta}{\partial t}=-\frac{1}{r}\frac{\partial}{\partial r}rv_rv_\theta-\frac{\partial}{\partial p}\omega v_\theta-\frac{v_\theta v_r}{r}-fv_r+K\left[\frac{1}{r}\frac{\partial}{\partial r}\left(r\frac{\partial v_\theta}{\partial r}\right)-\frac{v_\theta}{r^2}\right]+F_{tv} \tag{10}$$

where v_r and v_θ are the components of $\mathbf{V}$ in the radial and tangential directions, respectively, and F_{rv} and F_{tv} are the components of $\mathbf{F}_v$.

The isobaric height tendency at the earth's surface, which is assumed flat, is

$$\frac{\partial z}{\partial t}=\frac{\omega}{\rho g}-v_r\frac{\partial z}{\partial r}. \tag{11}$$

Since the fluid is autobarotropic, $\partial z/\partial t$ is independent of p.

The primitive equations (8)–(11) are integrated numerically to obtain v_r, v_θ, and ω at the 10 levels $p=100$, 200, . . ., 1000 mb. The pressure gradient force, obtained from (11), does not vary with height. In equation (11), ω is the value at the earth's surface rather than at 1000 mb. This is obtained by extrapolating the values at 900 and 1000 mb. The Coriolis parameter is assigned a constant value of 10^{-4} sec^{-1}. The forces F_{rv} and F_{tv} are zero except at 1000 mb. Here they are given by

$$F_{rv}=-C\rho v_rV/\Delta p$$

and

$$F_{tv}=-C\rho v_\theta V/\Delta p \tag{12}$$

where C is the drag coefficient, $V=(v_r^2+v_\theta^2)^{1/2}$ is the wind speed at 1000 mb, and $\Delta p=100$ mb. Equations (12) are applied at every grid point except the outer wall ($r=1000$ km). The value $K=4\times10^9$ cm^2 sec^{-1} is used. This lies within the range of values computed by Grimminger (1941) and Murgatroyd (1969). The frictional terms in equations (9) and (10) are computed from data at the previous rather than the current time step to avoid computational instability.

The horizontal mesh size Δr is 100 km and the time step is 5 min. Simple centered differences are used in general. For example,

$$\left(\frac{1}{r}\frac{\partial\psi}{\partial r}\right)_{r=r_i}=\frac{1}{r_i}\frac{\psi_{i+1}-\psi_{i-1}}{2\Delta r} \tag{13}$$

where the subscript denotes the grid point. One-sided differences are used for the second term in equation (8) in computing ω at $r=0$ and $r=1000$ km. However, the predicted values of z at the outer wall (1000 km) are too low when this value of ω is used in equation (11). This is remedied by extrapolating z linearly from values at $r=800$ and $r=900$ km.

The initial values of $z(r)$ at 1000 mb are given in figure 1. They are proportional to r^2 and correspond to a uniform initial geostrophic relative vorticity of 5×10^{-5} sec^{-1}. The initial velocities are given by

$$v_r=\omega=0 \tag{14}$$

and

$$\frac{v_\theta^2}{r}+fv_\theta-g\frac{\partial z}{\partial r}=0. \tag{15}$$

Thus, v_θ initially satisfies the gradient wind equation and is given in table 1. Throughout the integrations, v_θ is constrained to satisfy equation (15) at the outer wall and is, therefore, independent of p there. Other boundary conditions are

$$v_r=v_\theta=0 \text{ at } r=0$$

and

$$v_r=0 \text{ at } r=1000 \text{ km}. \tag{16}$$

Numerical integrations with the same initial conditions are carried out for 24 hr using the following values of the drag coefficient: 0, 5×10^{-4}, 2×10^{-3}, and 1×10^{-2} (figs. 1–7). In each case, C is increased linearly with time from zero initially to the above values by 72 time steps (6 hr). After 6 hr, C is held fixed. This procedure is preferable to imposing surface friction impulsively at the start. In the latter case, small-scale oscillations contaminate the results. Presumably this is important in the initialization procedure for any primitive equations model incorporating surface friction.

Predicted values of the tangential velocities after 24 hr, averaged over the 10 pressure levels, are presented in table 1. Typically, v_θ is constant from 100 to 900 mb, with a somewhat smaller value at 1000 mb. The loss in kinetic energy increases with r. Part of this is due to lateral diffusion, as is seen from the results for $C=0$. The most important reason, however, is that the surface stress varies as the square of the wind speed, and the latter increases with r.

Predicted values of $z(r)$ at 1000 mb after 24 hr are given in figure 1. In the case of $C=0$, the height changes are due to horizontal mixing. The height rises near the center

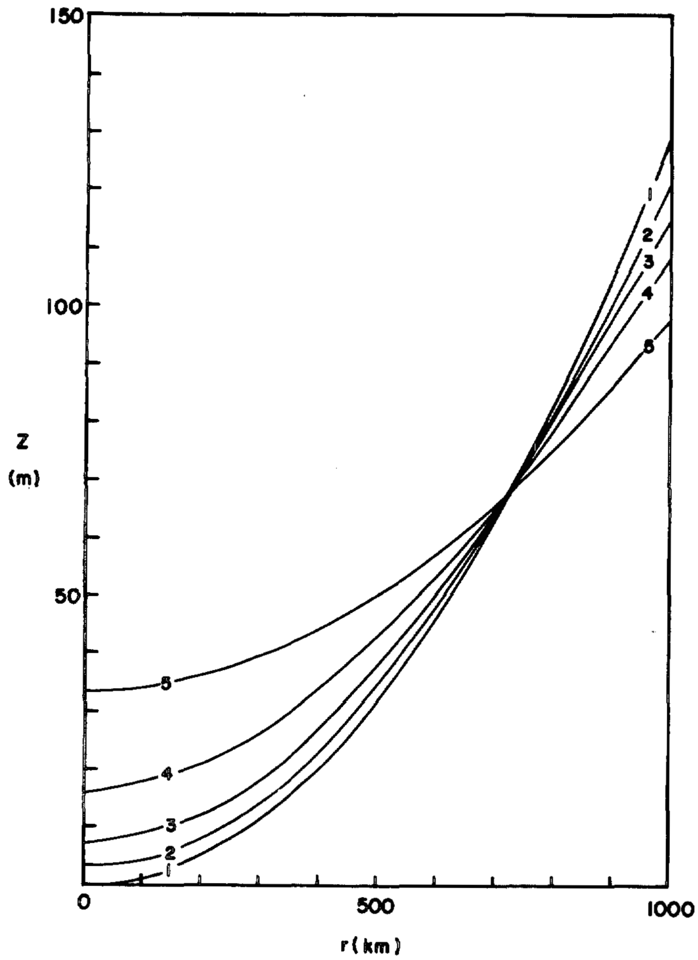

FIGURE 1.—Curve 1, initial values of $z(r)$ at 1000 mb; curves 2–5, 24-hr predicted values using $C=0$ (curve 2), 5×10^{-4} (curve 3), 2×10^{-3} (curve 4), and 1×10^{-2} (curve 5).

of the Low increase with the drag coefficient. The increase is somewhat less than linear.

The radial and vertical velocities are largest after about 10 hr. This is 4 hr after surface friction is fully imposed. Figures 2–7 show v_r and ω at this time for the non-zero values of the drag coefficient used. The magnitudes depend critically on the drag coefficient.

Under adiabatic conditions,

$$\Delta A+\Delta K=W \tag{17}$$

where A is the available potential energy of the fluid (Lorenz, 1955), K is the kinetic energy of the horizontal motion, Δ refers to a change over a time period Δt, and

$$W=\int_0^{\Delta t}\int_M \mathbf{V}\cdot\mathbf{F}dmdt \tag{18}$$

is the work done by friction. In equation (18), dm is an element of mass, M is the total mass, and $\mathbf{F}=K\nabla^2\mathbf{V}+\mathbf{F}_v$.

As shown in the appendix,

$$\Delta A=C_3S\Delta\overline{(z_0-\bar{z}_0)^2} \tag{19}$$

TABLE 1.—*Initial tangential velocities and average values after 24 hr (units, m sec^{-1})*

r(10^2 km)	Initial values	Values after 24 hr			
		$C=0$	$C=5\times10^{-4}$	$C=2\times10^{-3}$	$C=1\times10^{-2}$
0	0.0	0.0	0.0	0.0	0.0
1	2.0	2.1	2.0	1.8	1.3
2	4.4	4.2	4.0	3.6	2.6
3	6.1	6.2	6.0	5.3	3.6
4	8.1	8.3	7.8	6.9	4.7
5	10.5	10.2	9.6	8.4	5.6
6	12.6	12.1	11.3	9.7	6.6
7	14.6	13.8	12.7	10.8	7.7
8	16.6	15.1	13.8	11.7	8.8
9	18.7	16.2	14.5	12.4	9.6
10	19.7	16.9	14.7	12.6	10.0

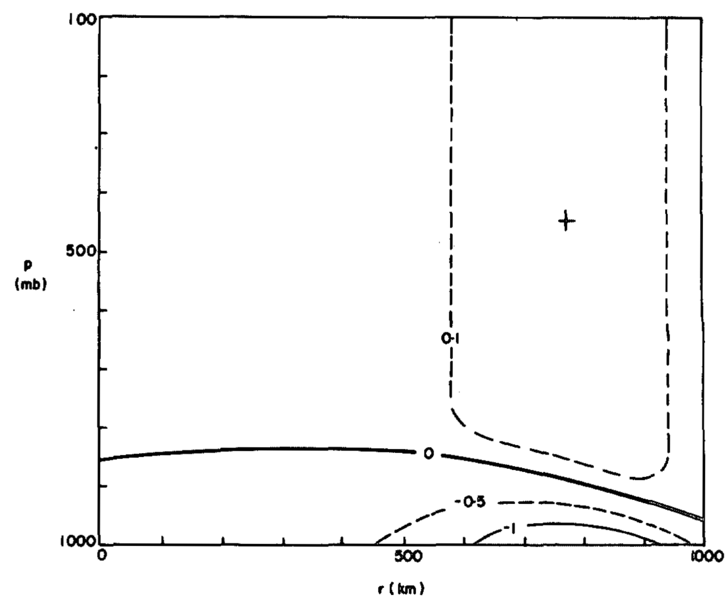

FIGURE 2.—Radial velocities after 10 hr for $C=5\times10^{-4}$ (units, m sec^{-1}).

where

$$C_3=\frac{C_p}{R}\rho_0\frac{g}{2}. \tag{20}$$

The bar denotes an average over the horizontal area S, and z_0 and ρ_0 are the height and density at the isobaric surface $p=1000$ mb.

The left side of equation (17) is evaluated from the results of the four numerical integrations described above (table 2). Here, $\Delta t=24$ hr. W is simply the sum of ΔA and ΔK and is not computed independently. Although K is considerably larger than A, the relative decrease $-\Delta A/A$ increases with increasing C somewhat faster than the ratio $-\Delta K/K$. Even though the frictional forces of equation (12) are directly proportional to C, the variation of $-W$ with C is less than linear. This is because the velocities at a given time decrease with increasing C. This is partially offset by the fact that the contribution of lateral mixing to $-W$ decreases with increasing C for the same reason.

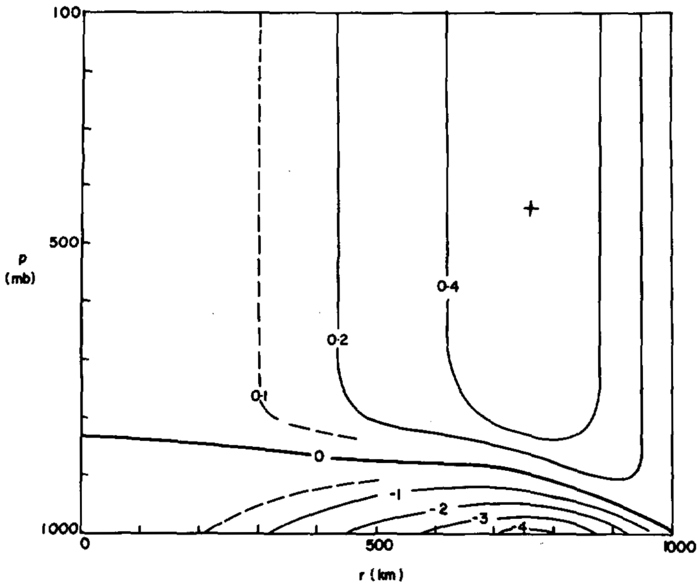

Figure 3.—Radial velocities after 10 hr for $C=2\times10^{-3}$ (units, m sec^{-1}).

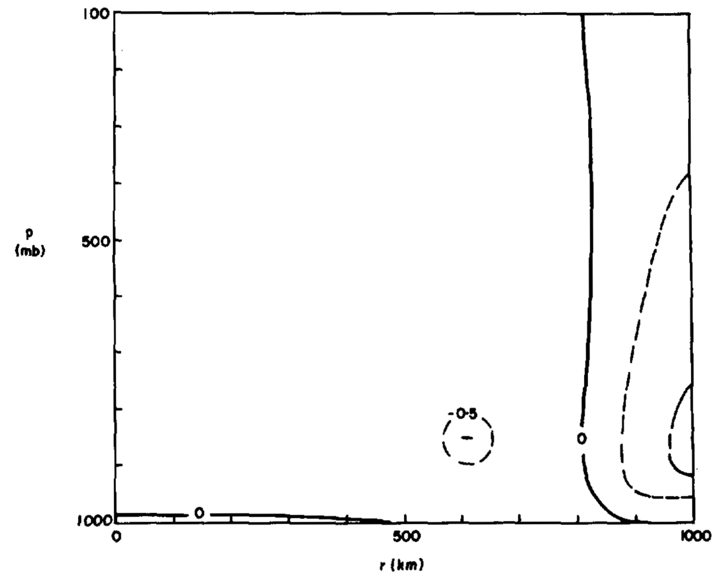

Figure 5.—Vertical velocities after 10 hr for $C=5\times10^{-4}$ (units, 10^{-3} mb sec^{-1}).

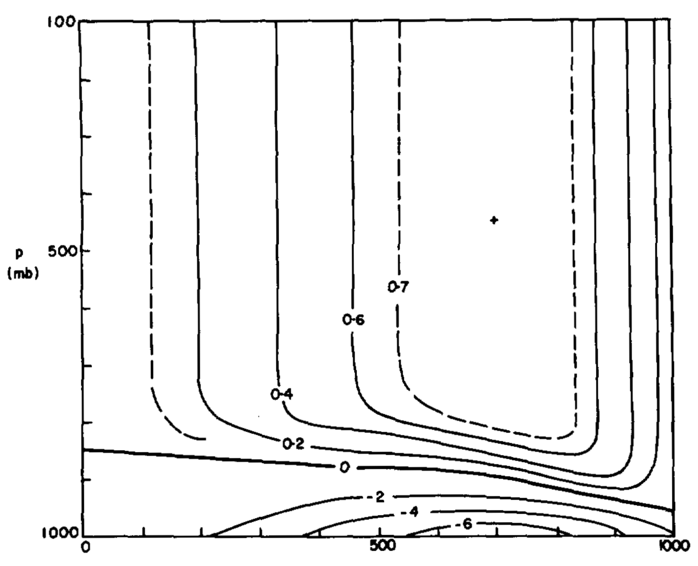

Figure 4.—Radial velocities after 10 hr for $C=1\times10^{-2}$ (units, m sec^{-1}).

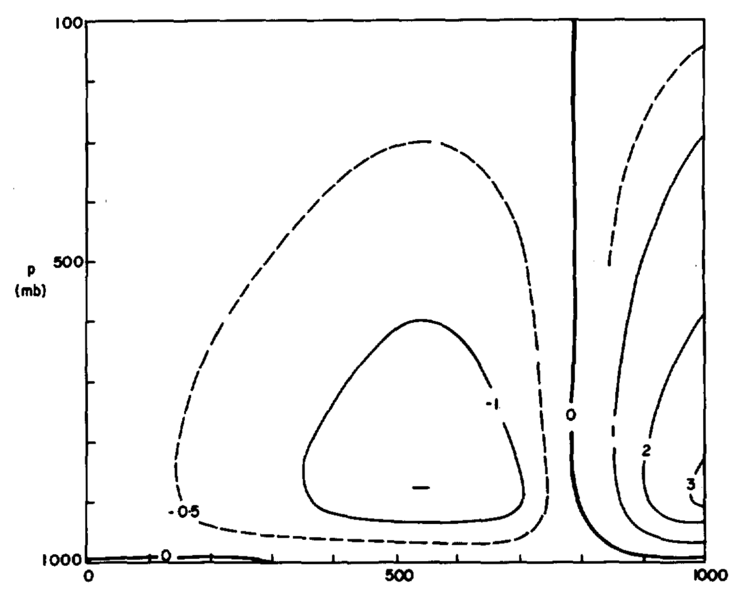

Figure 6.—Vertical velocities after 10 hr for $C=2\times10^{-3}$ (units, 10^{-3} mb sec^{-1}).

4. EXPERIMENTS WITH A QUASI-GEOSTROPHIC NUMERICAL MODEL

A more realistic study may be made using a numerical model incorporating effects of released latent heat. The author (Danard 1966*a*, *b*) has previously described such a model. This model uses the quasi-geostrophic vorticity and omega equations. Influences of orography and surface friction are included in the boundary condition for ω at 1000 mb. Here, the frictionally induced vertical velocity is prescribed by

$$\omega_f = -\frac{g}{\alpha f}\mathbf{k}\cdot\nabla\times C_g V_g \mathbf{V}_g. \tag{21}$$

The upper boundary condition is $\omega=0$ at 200 mb. With these boundary conditions, the omega equation is solved for vertical velocities at 775, 600, and 400 mb. The vorticity equation gives prognostic heights at 850, 700, 500, and 300 mb. The 1000-mb height is obtained from a linear relationship with the 850- and 700-mb heights.

The model is applied to two actual synoptic cases of cyclogenesis (figs. 8–15). For each case, four 36-hr integrations are performed:

1) moist with surface friction,
2) moist without surface friction,
3) dry with surface friction, and
4) dry without surface friction.

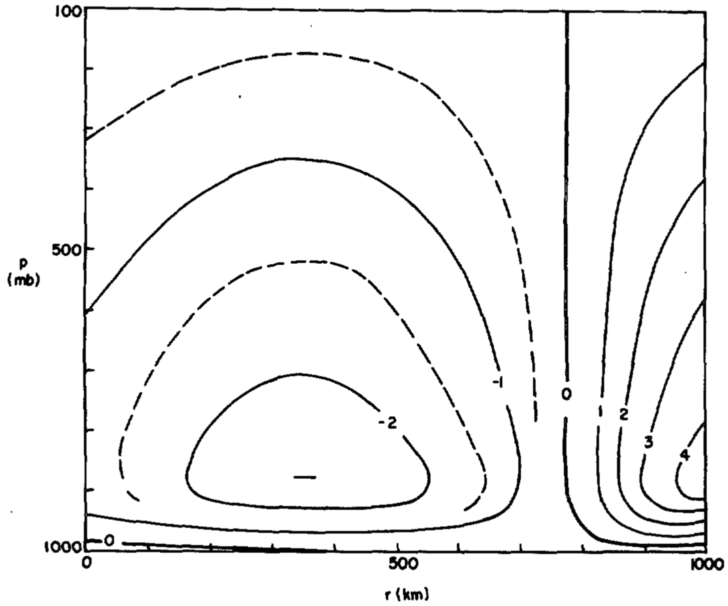

FIGURE 7.—Vertical velocities after 10 hr for $C=1\times10^{-2}$ (units, 10^{-3} mb sec^{-1}).

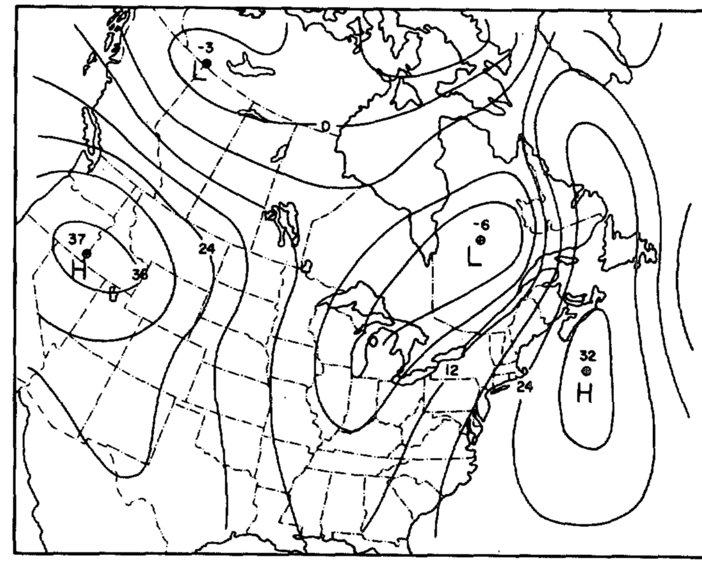

FIGURE 8.—The 36-hr 1000-mb prognosis for case 1 (valid for 0000 GMT on Feb. 13, 1965); moist without surface friction (units, 10 m).

TABLE 2.—*Initial values of K and A and 24-hr decreases, see equation (17). Units, 10^{24} ergs*

Initial values K	A	24-hr decreases			
6.9	1.9	$C=0$	$C=5\times10^{-4}$	$C=2\times10^{-3}$	$C=1\times10^{-2}$
$-\Delta A$		0.3	0.5	0.9	1.4
$-\Delta K$		1.2	2.2	3.5	5.0
$-W$		1.5	2.7	4.4	6.4
$-\Delta A/A$		0.18	0.33	0.58	0.86
$-\Delta K/K$		0.18	0.32	0.50	0.73

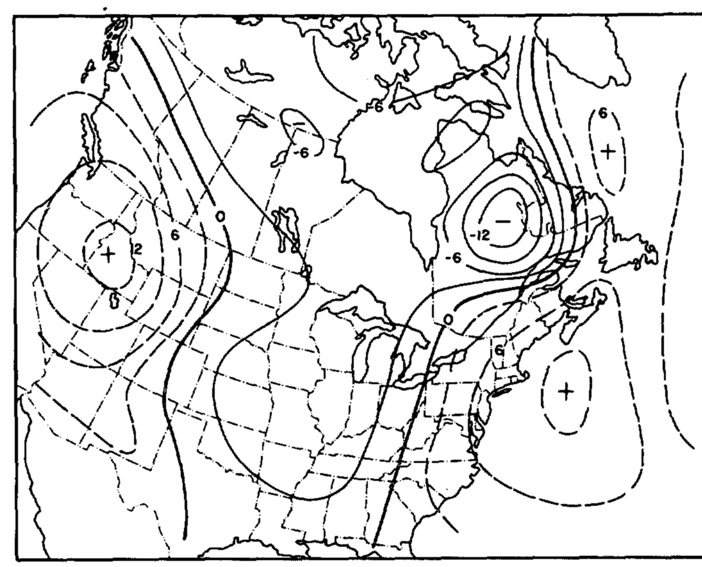

FIGURE 9.—Difference between 1000-mb moist prognoses (without friction-with friction) for case 1 (units, 10 m).

In the "moist" integrations, latent heat is released and precipitation amounts are predicted. In the "dry" mode, no condensation occurs during the computations. The calculations with surface friction use values by Cressman (1960) for the geostrophic drag coefficient C_g. These vary spatially. Surface friction is excluded simply by setting $C_g=0$ in equation (21).

The initial times for the two cases studied are 1200 GMT on Feb. 11, 1965, and 1200 GMT on Feb. 24, 1965. For convenience, these will be referred to as cases 1 and 2, respectively. The verifying 1000-mb chart for case 2 is given in figure 16. Results of the integrations including surface friction are given in Danard (1966*b*). From figures 8–15 of the present paper, it is seen that the exclusion of surface friction results mainly in more intense Highs and Lows. In the moist integrations, the precipitation center is moved faster when friction is excluded than it is when friction is included. This accentuates the trough northeast of the predicted low center (figs. 8 and 12) and accounts for the greater discrepancy there for the moist integrations (figs. 9 and 13).

As is evident in table 3, the root-mean-square difference between predictions with and without surface friction is a significant fraction of Δz at 1000 mb. The rms difference decreases with height up to 500 mb. Since Δz increases with height, the relative effect of surface friction decreases fairly rapidly. When release of latent heat is included, the differences increase. The chief reason is that in the "moist" integrations, the trough northeast of the cyclone center is affected more by surface friction than it is in the "dry" prognoses (see above discussion).

Surface friction has little overall effect on the predicted precipitation amounts. Predicted values for the integrations with surface friction as well as observed amounts are

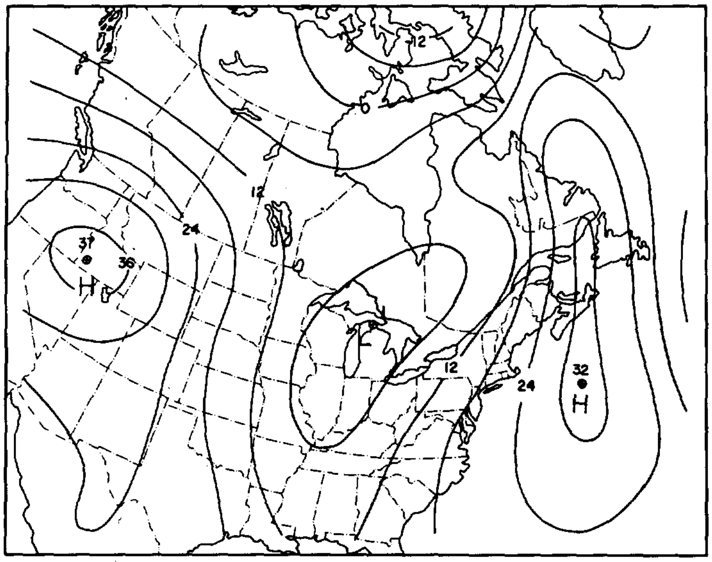

FIGURE 10.—The 36-hr 1000-mb prognosis for case 1; dry without surface friction (units, 10 m).

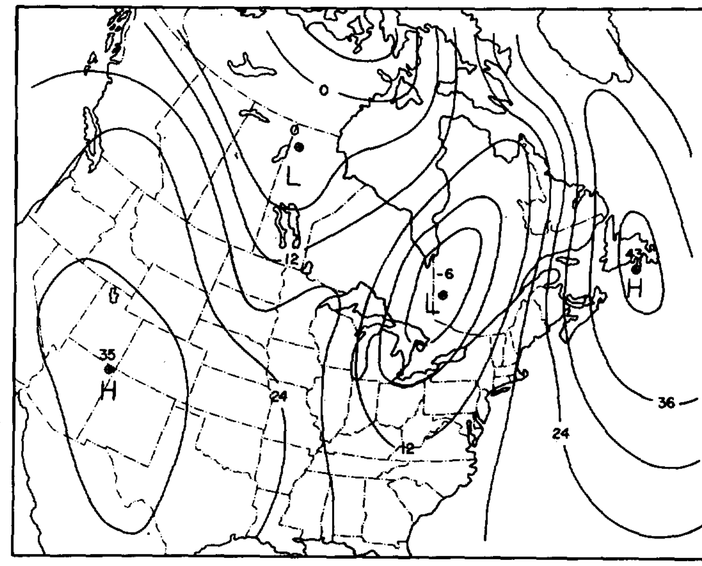

FIGURE 12.—The 36-hr 1000-mb prognosis for case 2 (valid for 0000 GMT on Feb. 26, 1965); moist without surface friction (units, 10 m).

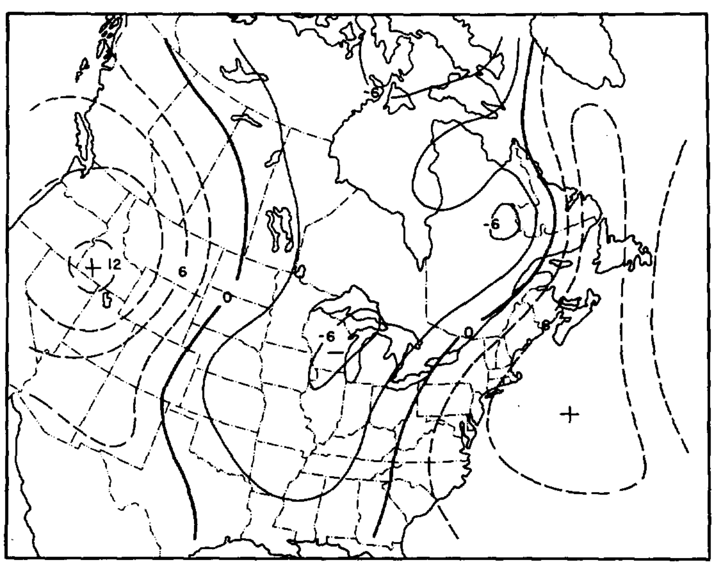

FIGURE 11.—Difference between 1000-mb dry prognoses (without friction-with friction) for case 1 (units, 10 m).

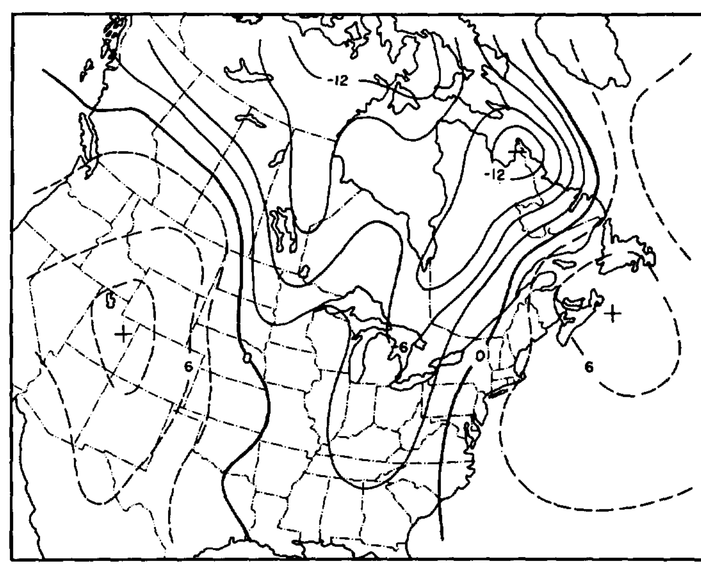

FIGURE 13.—Difference between 1000-mb moist prognoses (without friction-with friction) for case 2 (units, 10 m).

given in figures 11 and 12 of Danard (1966*b*). The totals for the area depicted in figures 8–15 of the present paper are shown in table 4. When surface friction is included, the cyclones are less intense and, presumably, midtropospheric vertical velocities are smaller. However, this is offset by the increase in low-level vertical velocity due to frictional convergence.

5. A COMPARISON OF TWO METHODS OF COMPUTING SURFACE STRESS

Cressman (1960) computes the surface stress from the equation

$$\tau_c = \rho C_g V_g^2 \tag{22}$$

where C_g is calculated from variations in height of terrain.

On the other hand, Kung (1966) proposes the following relation:

$$\tau_k = \rho C_k^2 V_g^2. \tag{23}$$

Here, C_k is obtained from a regression equation using tabulated values by Lettau (1962) as a function of surface Rossby number Ro_s:

$$\mathrm{Ro}_s = \frac{V_g}{z_0 f} \tag{24}$$

and

$$C_k = \frac{0.205}{\log_{10} \mathrm{Ro}_s - 0.556}. \tag{25}$$

The roughness parameter z_0 is determined by the vegeta-

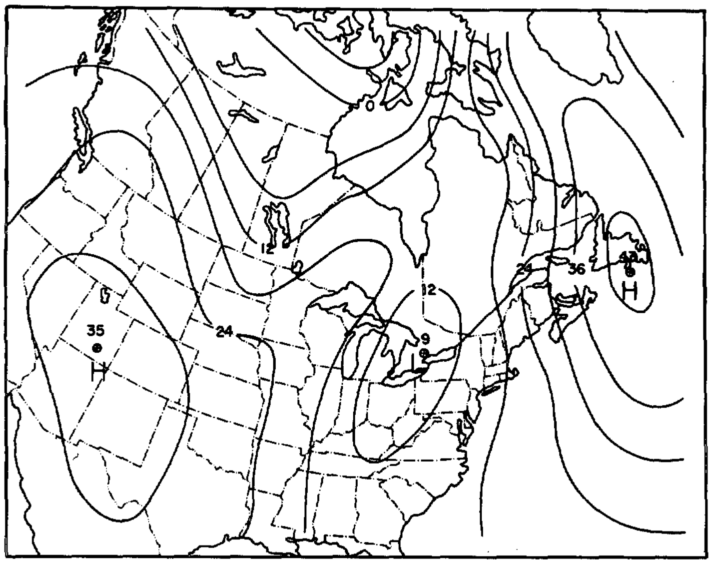

FIGURE 14.—The 36-hr 1000-mb prognosis for case 2; dry without surface friction (units, 10 m).

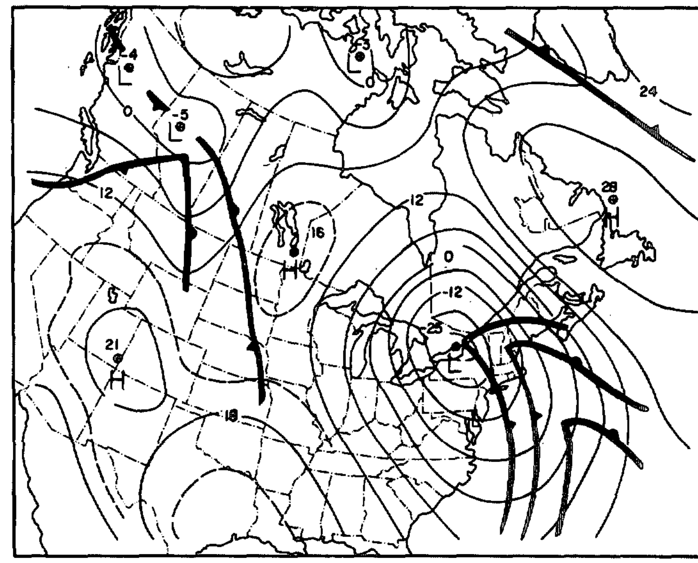

FIGURE 16.—The 1000-mb chart for 0000 GMT on Feb. 26, 1965 (units, 10 m).

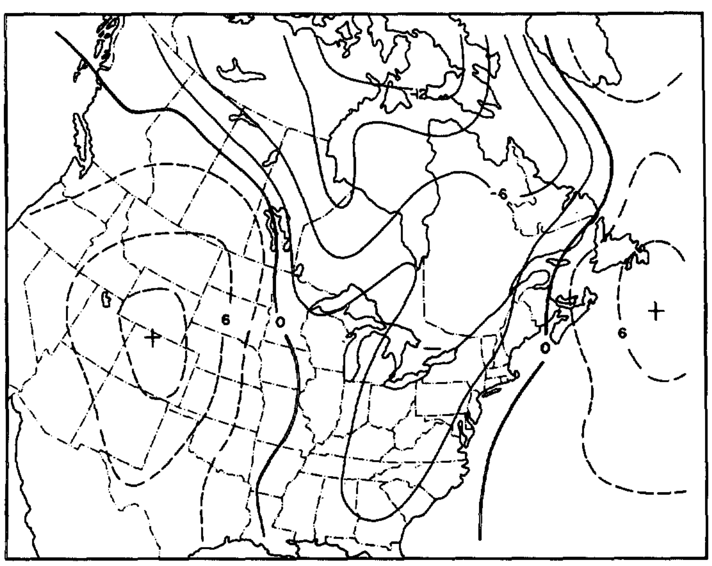

FIGURE 15.—Difference between 1000-mb dry prognoses (without friction-with friction) for case 1 (units, 10 m).

TABLE 3.—*Root-mean-square height differences between 36-hr numerical predictions with and without surface friction. Δz is the actual rms 36-hr height change (units, meters)*

Level (mb)	Case 1			Case 2		
	Moist	Dry	Δz	Moist	Dry	Δz
1000	54	50	72	59	54	132
850	43	41	64	47	44	119
700	35	33	82	39	35	134
500	32	29	126	37	32	179
300	32	29	165	38	32	245

TABLE 4.—*Total 36-hr predicted precipitation for the area shown in figures 8–15 (units, 10^{16} gm)*

Case	1	2
With friction	4.7	6.9
Without friction	5.0	7.0

tion, without regard to orography. This is the most important difference between equations (22) and (23). However, it is not intended to imply that Kung was unaware of the significance of topography.

Figures 17 and 18 show the results of computing the surface stress by the two methods, Cressman's and Lettau and Kung's, for the synoptic case shown in figure 16. These computations were performed by Graham (1968). The lack of agreement between figures 17 and 18 is obvious, especially over the western part of North America. Thus it appears that our knowledge of the surface stress is still far from complete.

6. CONCLUDING REMARKS

When surface friction is imposed impulsively in the primitive equation integrations described in section 3, gravity waves result. This suggests that the initial velocities should take into account the same physical processes as the model itself. In the present study, this is remedied by introducing friction gradually during the first 6 hr.

Frictionally induced vertical velocities and pressure tendencies depend critically on the surface stress. However, the drag coefficient varies by two orders of magnitude over the earth's surface. It is, therefore, suggested that surface friction plays an important role in the dynamics of the atmosphere.

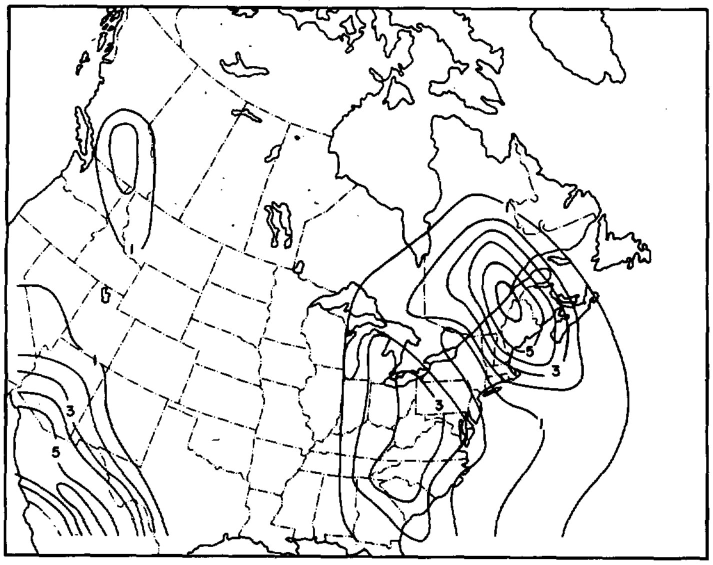

FIGURE 17.—Surface stress computed by Cressman's method (see equation (22)) for 0000 GMT on Feb. 26, 1965 (units, 10 dynes cm^{-2}).

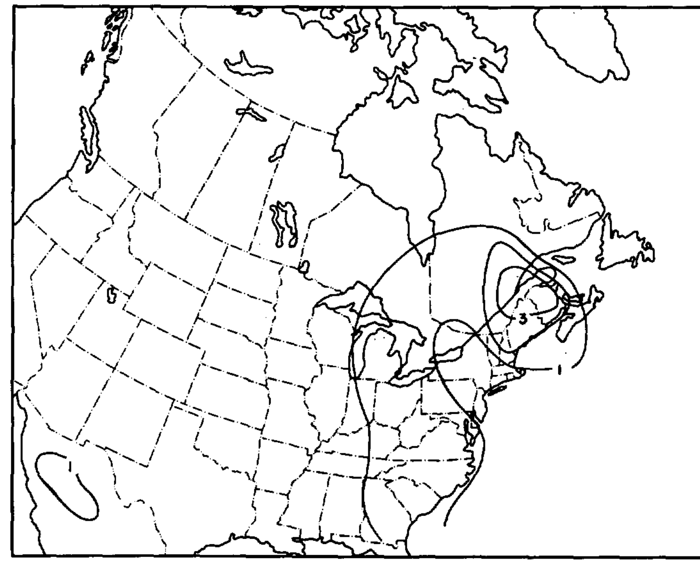

FIGURE 18.—Surface stress computed by Lettau and Kung's method, see equation (23), for 0000 GMT on Feb. 26, 1965 (units, 10 dynes cm^{-2}).

The effect on precipitation is not clear. Surface friction appears to inhibit cyclogenesis (see section 4) and, therefore, reduce midtropospheric vertical velocities. On the other hand, low-level vertical motions are enhanced by frictional convergence. Perhaps the best test would be comparative integrations with a multilevel primitive equations model using real initial data.

APPENDIX

DERIVATION OF EQUATION (19)

To derive an expression for A, we note that an autobarotropic atmosphere has a dry-adiabatic lapse rate γ_d and a depth T_s/γ_d, where T_s is the surface temperature. The total potential energy per unit area is

$$(P+I)=\int_0^{T_s/\gamma_d}(gz+C_vT)\rho dz=\frac{C_p}{R}\int_0^{T_s/\gamma_d}pdz. \quad (26)$$

Substituting $p=p_s\left(1-\frac{\gamma_d z}{T_s}\right)^{g/R\gamma_d}$ in equation (26) yields

$$(P+I)=\frac{C_pT_sp_s}{g+\gamma_dR}. \quad (27)$$

However,

$$p_s=p_0\left(1+\frac{\gamma_d z_0}{T_0}\right)^{g/R\gamma_d}$$

and (28)

$$T_s=T_0\left(1+\frac{\gamma_d z_0}{T_0}\right)$$

where z_0 and T_0 are the height and temperature at the isobaric surface $p_0=1000$ mb. Substituting (28) in (27) gives

$$(P+I)=\frac{C_pT_0p_0}{g+\gamma_dR}\left(1+\frac{\gamma_d z_0}{T_0}\right)^{(g/R\gamma_d)+1} \quad (29)$$

Omitting terms of higher order than z_0^2, equation (29) becomes

$$(P+I)=C_1+C_2z_0+C_3z_0^2 \quad (30)$$

where

$$C_1=\frac{C_pT_0p_0}{g+\gamma_dR},$$

$$C_2=\frac{C_pp_0}{R},$$

and (31)

$$C_3=\frac{C_p}{R}\rho_0\frac{g}{2}.$$

The area-averaged total potential energy, denoted by a bar, is

$$\overline{(P+I)}=C_1+C_2\overline{z}_0+C_3\overline{z_0^2}. \quad (32)$$

This has a minimum when $z_0=\overline{z}_0$ everywhere:

$$\overline{(P+I)}_{min}=C_1+C_2\overline{z}_0+C_3\overline{z}_0^2.$$

The available potential energy is just the difference multiplied by the area S:

$$A=C_3(\overline{z_0^2}-\overline{z}_0^2)S=C_3\overline{(z_0-\overline{z}_0)^2}S. \quad (33)$$

For use in equation (17), we have

$$\Delta A=C_3S\Delta\overline{(z_0-\overline{z}_0)^2} \quad (34)$$

where $\overline{z}_0$ is invariant for an adiabatic autobarotropic fluid.

ACKNOWLEDGMENTS

This research was supported by the National Research Council of Canada. The author wishes to express his thanks to Mr. Stanley Alleyne for assistance in running the computer programs, to Mrs. Jackie Chen for drafting the figures, and to Mrs. Olga Roehrig for typing the manuscript.

REFERENCES

Bushby, F., "Further Developments of a Model for Forecasting Rain and Weather," paper presented at the WMO/IUGG Symposium on Numerical Weather Prediction, Tokyo, Nov. 26–Dec. 4, **1968**.

Charney, J. G., and Eliassen, A., "On the Growth of the Hurricane Depression," *Journal of the Atmospheric Sciences*, Vol. 21, No. 1, Jan. **1964**, pp. 68–75.

Cressman, G. P., "Improved Terrain Effects in Barotropic Forecasts," *Monthly Weather Review*, Vol. 88, Nos. 9–12, Sept.–Dec. **1960**, pp. 327–342.

Danard, M. B., "On the Influence of Released Latent Heat on Cyclone Development," *Journal of Applied Meteorology*, Vol. 3, No. 1, Feb. **1964**, pp. 27–37.

Danard, M. B., "A Quasi-Geostrophic Numerical Model Incorporating Effects of Released Latent Heat," *Journal of Applied Meteorology*, Vol. 5, No. 1, Feb. **1966*a***, pp. 85–93.

Danard, M. B., "Further Studies With a Quasi-Geostrophic Numerical Model Incorporating Effects of Released Latent Heat," *Journal of Applied Meteorology*, Vol. 5, No. 4, Aug. **1966*b***, pp. 388–395.

Graham, I., "Calculations of Surface Stress," U.S. Naval Postgraduate School, Monterey, Calif., **1968**, 16 pp., (unpublished).

Graystone, P., "The Introduction of Topographic and Frictional Effects in a Baroclinic Model," *Quarterly Journal of the Royal Meteorological Society*, Vol. 88, No. 377, July **1962**, pp. 256–270.

Grimminger, G., "The Intensity of Lateral Mixing in the Atmosphere As Determined From Isentropic Charts," *Bulletin of the American Meteorological Society*, Vol. 22, No. 5, May **1941**, pp. 227–233.

Holopainen, E. O., "On the Dissipation of Kinetic Energy in the Atmosphere," *Tellus*, Vol. 15, No. 1, Feb. **1963**, pp. 26–32.

Krishnamurti, T. N., "A Calculation of Percentage Area Covered by Convective Clouds From Moisture Convergence," *Journal of Applied Meteorology*, Vol. 7, No. 2, Apr. **1968**, pp. 184–195.

Kung, E. C., "Kinetic Energy Generation and Dissipation in the Large-Scale Atmospheric Circulation," *Monthly Weather Review*, Vol. 94, No. 2, Feb. **1966**, pp. 67–82.

Kung, E. C., "On the Momentum Exchange Between the Atmosphere and the Earth Over the Northern Hemisphere," *Monthly Weather Review, Vol.* 96, No. 6, June **1968**, pp. 337–341.

Kuo, H.-L., "On Formation and Intensification of Tropical Cyclones Through Latent Heat Release by Cumulus Convection," *Journal of the Atmospheric Sciences*, Vol. 22, No. 1, Jan. **1965**, pp. 40–63.

Lettau, H. H., "Theoretical Wind Spirals in the Boundary Layer of a Barotropic Atmosphere," *Beiträge zur Physik der Atmosphäre*, Vol. 35, No. 3/4, Frankfurt, **1962**, pp. 195–212.

Lorenz, E. N., "Available Potential Energy and the Maintenance of the General Circulation," *Tellus*, Vol. 7, No. 2, May **1955**, pp. 157–167.

Murgatroyd, R. J., "Estimations From Geostrophic Trajectories of Horizontal Diffusivity in the Mid-Latitude Troposphere and Lower Stratosphere," *Quarterly Journal of the Royal Meteorological Society*, Vol. 95, No. 403, Jan. **1969**, pp. 40–62.

Ooyama, K., "A Dynamical Model for the Study of Tropical Cyclone Development," *Geofisica Internacional*, Vol. 4, No. 4, Oct. **1964**, pp. 187–198.

Sawyer, J. S. "The Introduction of the Effects of Topography Into Methods of Numerical Forecasting," *Quarterly Journal of the Royal Meteorological Society*, Vol. 85, No. 363, Jan. **1959**, pp. 31–43.

Sheppard, P. A., "Transfer Across the Earth's Surface and Through the Air Above," *Quarterly Journal of the Royal Meteorological Society*, Vol. 84, No. 361, July **1958**, pp. 205–224.

Shuman, F. G., and Hovermale, J. B., "An Operational Six-Layer Primitive Equation Model," *Journal of Applied Meteorology*, Vol. 7, No. 4, Aug. **1968**, pp. 525–547.

Smagorinsky, J., Manabe, S., and Holloway, J. L., Jr., "Numerical Results From a Nine-Level General Circulation Model of the Atmosphere," *Monthly Weather Review*, Vol. 93, No. 12, Dec. **1965**, pp. 727–768.

[Received April 28, 1969; revised June 16, 1969]